Space Sci Rev
DOI 10.1007/s11214-008-9346-z

Blue Jets: Upward Lightning

Evgeny V. Mishin · Gennady M. Milikh

Received: 12 December 2007 / Accepted: 25 March 2008

Abstract Blue jets are beams of blue light propagating from the tops of active thunderclouds up to altitudes of ∼50 km. They resemble tall trees with quasi-vertical trunk and filamentary branches. Their apparent speeds are in the range of 10 s to 100 s km/s. Other events, having essentially lower terminal altitudes (<26 km), are named blue starters. These phenomena represent the first documented class of upward electrical discharges in the stratosphere. Some of upward discharges, termed gigantic jets, propagate into the lower ionosphere at much higher speeds in the final phase. We describe salient features of the upward discharges in the atmosphere, give an assessment of the theories of their development, and discuss the consequences for the electrodynamics and chemistry of the stratosphere. We argue that this upward lightning phenomenon can be understood in terms of the bi-directional leader, emerging from the anvil.

Keywords Blue jets · Upward lightning · Transient discharges · Bi-leader

1 Introduction

Luminous flashes above thunderstorms have been reported by eyewitnesses for over a century (e.g., see review Vaughan and Vonnegut 1989) and eventually documented from low-light optical observations on the ground (Franz et al. 1990; Lyons 1994), airborne platforms (Sentman and Wescott 1993), and the space shuttle (Vaughan et al. 1992). However, only during the Sprites94 aircraft campaign Wescott et al. (1995) identified the class of upward-propagating stratospheric flashes, named blue jets (BJ) due to primarily blue color, as opposed to the red-color sprites at mesospheric altitudes (Sentman et al. 1995). Brief upward

E.V. Mishin (✉)
Boston College, Chestnut Hill, MA, USA
e-mail: evgenii.mishin@hanscom.af.mil

G.M. Milikh
University of Maryland, College Park, MD, USA
e-mail: milikh@umd.edu

jets, which propagate only a few km and terminate below 26 km, were dubbed blue starters (BS) (Wescott et al. 1996). A number of BJ/BS and similar events were captured during the ground and aircraft observations (Wescott et al. 1998, 2001); Lyons et al. 2000, 2003) and apparently from the space shuttle (Boeck et al. 1995, 1998). Pasko et al. (2002) and Su et al. (2003) discovered the so-called gigantic jets (GJ), propagating into the mesosphere/lower ionosphere (6 events). Recently, eight GJ events have been identified from the imager ISUAL onboard Formosat-2 (Kuo et al., *Workshop on streamers, sprites, leaders, lightning: From micro- to macro-scales*, Leiden, 2007).

The BJ/BS phenomena were quickly recognized as manifesting upward transient discharges in the stratosphere. Earlier BJ theories included the runaway breakdown (Roussel-Dupré and Gurevich 1996) and streamers of the positive (Pasko et al. 1996) and negative (Sukhorukov et al. 1996) polarity as the underlying physical mechanisms (see reviews Sukhorukov and Stubbe 1998; Rowland 1998). As the streamer models require seemingly extreme conditions, Sukhorukov and Stubbe (1998) and Petrov and Petrova (1999) suggested that BJ is rather formed by the streamer corona of a leader. This idea was further explored by Pasko and George (2002), who numerically simulated the streamer corona of a positive leader as a stochastic (fractal) process. However, likewise customary cloud to ground (CG) lightning, single-headed leaders require unrealistic rates of the thundercloud charge transport. To clear this hurdle, Raizer et al. (2006, 2007) suggested that the bi-directional uncharged leader (Kasemir 1960) forms in the anvil. As the leader channel transfers the thundercloud potential upward, the overall growth can be maintained by fairly moderate cloud charges and currents.

We next present the salient features of BJ/GJ (or Jets) and related upward discharges, then discuss theory of their evolution and consequences for the electrodynamics and chemistry of the upper atmosphere. We do not dwell on theoretical details, describing the underlying physical processes and basic limitations on a semi-qualitative level, just sufficient for comparison with the observations.

2 Observations of Upward Discharges in the Atmosphere

2.1 Blue Jets and Blue Starters

Four consecutive video frames, 67 ms apart, in Fig. 1 adapted from Wescott et al. (1996) (hereafter referred to as W96) shows the typical BJ development over continental thunderstorms. Note that hereafter the images (most in false color) are adjusted to show the faint

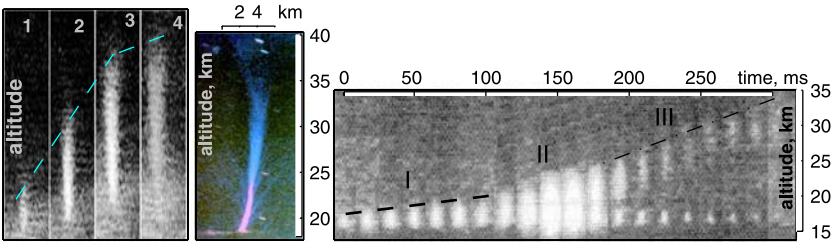

Fig. 1 (*Left*) Four video frames, 67 ms apart, during the 4 July 1994 BJ event from the Westwind 2 aircraft. (*Middle*) A 2-min exposure color photograph (in false color) of a blue jet north of Réunion Island and (*right*) a 350-ms sequence of narrow field TV images (16.67 ms apart) of the 22 July 1998 BJ event captured during the EXL98 aircraft campaign (adapted from W01). *Dashed lines* mark the BJ tip. Reprinted by permission from the American Geophysical Union

features and then annotated. One can see a slightly-conical ($\sim$10° angle) jet propagating upward out of the top of the anvil at a $\simeq$100-km/s speed to a terminal altitude of $\sim$40 km. Hereafter, 'speeds' designate 'apparent vertical speeds'. Note that the jet in frame 1 nearly resembles a dim starter (cf. Fig. 1 W96 and Fig. 5 Lyons et al. 2003 (L03)). Near the terminus, the jet decelerated and its brightness seems to decay along the column simultaneously.

The next two frames show BJ over the Indian Ocean and over Iowa, respectively (Wescott et al. 2001 (W01)). The 'oceanic' BJ resembles a tree with filamentary branches (streamers) in the lower part and a forked tip crowned with two faint prongs (evident in Fig. 1 W01). An apparent diameter at the base is $\sim$400 m and broadens to $\sim$2 km at an altitude $h \simeq 30$ km, whereas the lower branches are $\sim$50–100 m wide (W01). The brightest, pencil-like lower part appears white due to saturation of the film, whilst the upper conical part is blue (cf. Fig. 3–4 L03). W01 found that the brightness of a saturated pixel exceeds 6.7 MR and that they account for $\simeq$25% of the total (blue) optical energy of $\geq$0.5 MJ. Assuming the jet duration 0.25 s yields the total optical power $\geq$2 MW.

The jet development can change abruptly. Indeed, the stage I in the right frame of Fig. 1 resembles a 'persistent' starter propagating upward at $\simeq$23 km/s. Then it suddenly brightened (II) and finally separated into two parts (III). The lower part shrinks to the origination point, while the upper streak continues upward at $\sim$90 km/s, disappearing from sight at $h \sim 35$ km. Note that a number of starters were also detected during the EXL98 campaign (W01). Multispectral video observations revealed that the second positive band 2PN2 contributed $\sim$90% to a $\sim$1-MR starter, whilst the flux of 427.8-nm photons amounted to $\sim$10 kR. This indicates the huge ionization rate.

Finally, L03 reported on observations by the ultrablue LLTV system of 83 very small ($\sim$100-m in size), $<$16-ms duration, bright 'pixies' and of 17 compact ($<$1-km) bright starters ('gnomes') during a 20-min period of rapid vertical development of a convective dome near Yucca Ridge, Kansas. The overall observations show that (1_b) BJ/BS and gnomes/pixies are not coincident with CG flashes of either polarity, (2_b) the BJ/BS speeds are in the range of $\sim$25–220 km/s, (3_b) the typical jet duration is $\sim$0.2–0.3 s at the base. Wescott et al. (1998) stressed an association of BS with very large hail; however, it does not seem to be a persistent feature, and (4_b) some jets seem to originate from the same location as preceding BS/BJ tens of ms apart.

2.2 Gigantic Jets

The bottom panel in Fig. 2 shows a $\sim$215-ms sequence of video fields at the beginning of the GJ event captured from the ground by Pasko et al. (2002 (P02)) on 15 September 2001 over the Atlantic Ocean. Evidently, the jet structure and apparent speed vary significantly from field to field. Initially (until field #11), the jet resembles two trunks (with faint branches) growing in step with the average speed $\sim$60 km/s. Further, the left trunk brightened and sped up to $\sim$200 km/s (#11–12), then decelerated (#12–13) and again brightened and accelerated to $\sim$500 km/s (#13–14). We designate this period of a 'smooth' average growth as stage A (cf. Fig. 1). At the beginning of stage B (#15), the upper part of the left trunk (beyond $\sim$30 km) strongly brightened. Its forked tip seems to have propagated to $\sim$48 km at $\sim$500 km/s and 'ejected' two prongs, which move at $\sim$1200 km/s and connect with bright diffuse spots at $h \sim 70$ km (cf. the GJ_4 #2$\rightarrow$#3 transition in the top panel). Except for the uppermost part, the structure resembles a tall version of the 'oceanic' BJ in Fig. 1 (cf. Fig. 10 Pasko and George 2002).

Meanwhile, the right trunk's tip (marked by dots), growing barely between #11–15, then 'exploded' in #16. Its wide and bright tip near 50 km is crowned with several prongs that

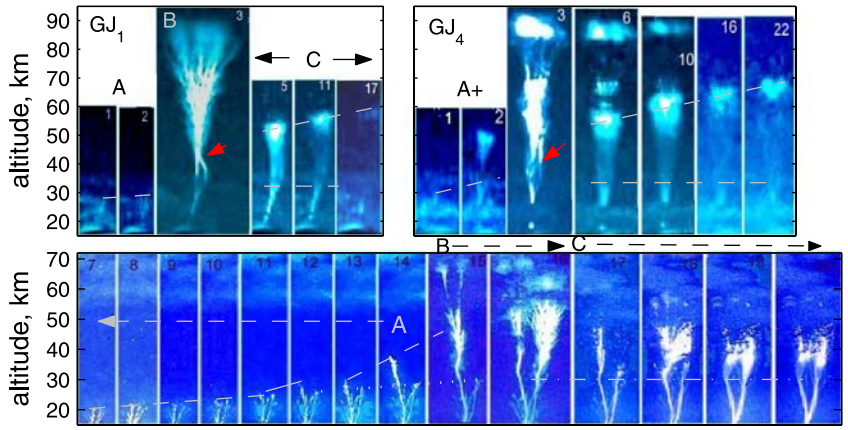

Fig. 2 (*Bottom*) Video fields 7-20 (∼17 ms each) during the 15 Sep 2001 GJ event ∼200 km northwest of Arecibo Observatory, Puerto Rico (adapted from P02 Suppl. Info.). (*Top*) Two sequences of video images (∼17 ms each) of the GJ events 1 (*left*) and 4 (*right*) on 22 July 2002 over the South China Sea (adapted from Su03). The red arrows mark apparent merging of two branches. Reprinted by permission from *Nature*

extend farther, mapping into a bright diffuse spot a few km above. Next (stage *C*), the uppermost spots faded away, whilst the forked structure at $h \leq 32$ km persisted for the rest of the event. The thick prongs appear Y-like (due to overlapping at the base) and connected via conical 'flare' with brighter diffuse tops between ∼35 and <50 km that occasionally brighten and expand. After #22 (see P02), the faint prongs and their brighter tops seem to decay in step. At low resolution, the overall decaying structure would appear consisting of a pencil-like trunk (emanating faint flare) and a diffuse top well apart (cf. stage III in Fig. 1). Rebrightening at seemingly the same location (cf. 4_b) occurs at #36 and forms a luminous structure alike stage *C* with the top at ∼50 km.

The top panel in Fig. 2 shows two GJ (Su et al. 2003 (Su03)) apparently emerging from the convective core. Su03 distinguished three stages of the GJ evolution: $^{(1)}$leading jet (#1–2), $^{(2)}$fully developed jet, and $^{(3)}$trailing jet. We estimate the speed of the tip (marked by the dashed line) in $GJ_1^{(1)}/GJ_4^{(1)}$ roughly to be ≥120/230 km/s. $GJ_4^{(1)}$ in #2 appears to comprise of a trunk below ∼32 km, and a structured upper part, propagating at ∼1000 km/s to ∼50 km (cf. the left jet below 50 km in the bottom #15–16). It seems to be the initial step in the $GJ_4^{(1)} \rightarrow GJ_4^{(2)}$ transition (cf. #15 in the bottom panel). $GJ_1^{(2)}$ in #3 and $GJ_4^{(2)}$ in #3–4 resemble a tall version of the right and left jet in #16 (bottom), respectively.

Notwithstanding their durations, the overall features of $GJ^{(1)}$ and $GJ^{(2)}$ are similar to stages *A* and *B* in the bottom panel, respectively. When stage *B* ends, there grows the trailing jet (cf. 4_b). Its structure, i.e. a trunk at the base connected via conical faint flare with diffuse top near 50–60 km (cf. rebrightening above), is alike the decaying $GJ_4^{(2)}$, except for a chute-shape region between 70 and 90 km. Note again that at low resolution $GJ^{(3)}$ would be reminiscent of stage III above. Overall, the leading and trailing jets seem nearly resembling the (enlarged) BJ. On the other hand, $GJ^{(2)}$ (stage *B*) seems to be distinguished by the upper luminous structures beyond the standard BJ terminus and their vivid dynamics. P02 stressed that these structures do not match the established sprite features.

In Fig. 2 red arrows mark the merging of two branches in $GJ_{1,4}^{(2)}$, which resembles those observed in laboratory streamers (Fig. 5b). Briels et al. (2006) explained the (electrostatic) attraction of two *non-conductive* streamers as consequent to a 'return stroke' piercing the early streamer. Cummer et al. (2006) suggested that a similar merging in sprites is due to

'mirror' charges induced in the *conductive* channel of the earlier streamer by the charged tip of the later streamer. We argue that the charge distribution in the long streamer (Fig. 7d) provides a natural explanation for the observed merging.

Finally, P02 reported on observations of VLF spherics of the positive polarity, coincident with the rebrightening event (trailing jet), and suggested negative cloud-to-ionosphere (−CI) breakdown to be their cause. Su03 detected ELF transients of the positive polarity during the GJ events and also interpreted as −CI discharges with the charge moment change 1–2 kC·km. However, there may be a slight chance that these transients were associated with +CG lightning in the nearby thunderstorm. If GJ were −CI discharges, each would remove about 30 C from the thundercloud and ionosphere, thereby decreasing the potential difference in the whole gap (Su03).

2.3 Jets and Lightning Activity

Likewise the BJ/BS family, the GJ events were not observed to be associated with preceding CG flashes of either polarity. Furthermore, they were detected mainly over oceans and shores where the rate of lightning flashes is low. This is evident in Fig. 3, where the locations of all known GJ events (red stars) are superimposed with the lightning distribution over the globe. Besides, black squares indicate some of eighty intense UV (300–400 nm) flashes, detected at ∼950 km onboard the student microsatellite 'Tatiana' (Garipov et al. 2005). They were almost equally distributed between two groups with durations 1–4 ms and 10–64 ms, corresponding to the lifetimes of individual streamers and of leaders, respectively (see below). Their radiated energy (∼0.1 MJ) is close to that from GJ (Su03). Thus, we suggest that these flashes are indicative of GJ. As it follows from Fig. 3, alike GJ, the UV flashes are detected mainly over regions with low CG/IC lightning activity.

The generation of locally-enhanced charges initiating Jets has not yet been understood. The charge distribution in the thundercloud depends on various processes, including CG and IC activity (e.g., Stoltzenburg and Marshal 2008). Sukhorukov et al. (1996) noted that Jets should be linked to exceptional thunderstorm conditions and suggested that long IC 'spiders', which are usually missed by the NLDN, can collect enough (negative) charge in the anvil. However, as Fig. 3 shows, this is unlikely during the GJ and UV events. Nor does there appear to be any clear relationship of IC lightning to brief discharges arising out of the anvil mostly during quiet intervals (W96; L03).

W96 have found that following a starter the average rate of nearby −CG flashes drops shortly by a factor of 5 and resumes in ≈3 s (a 2-s gap is found for BJ). In our opinion, this in-

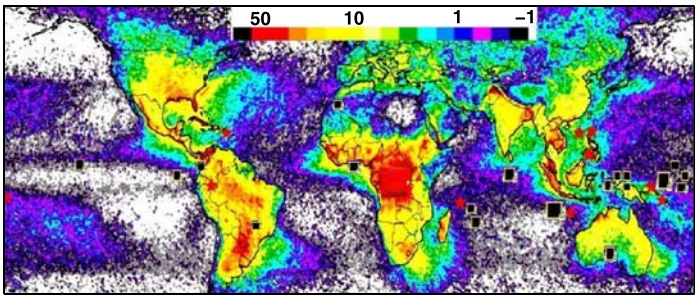

Fig. 3 Global lightning map (http://thunder.nsstc.nasa.gov/data/query/2004) with superimposed locations of the GJ events (stars) and ≤64-ms, ≤0.1-MJ, 300–400-nm UV flashes (*squares*) from the student microsatellite 'Tatiana' (Garipov et al. 2005)

dicates that −CG flashes and BJ/BS 'compete' for the same source (cf. Pasko et al.'s (1996) pre-discharge concept). By the same token, we suggest that GJ 'prefer' oceanic storms as highly-conductive sea water cannot maintain pointed 'towers', which initiate CG lightning in continental storms. Note that initiation of the conventional breakdown inside a cloud poses a serious problem as the observations (e.g., Bazelyan and Raizer 2000 (BR00); Stoltzenburg and Marshal 2008) show that electric fields very seldom exceed a few kV/cm. It is well below the threshold value $E_{th} = \eta \cdot E_{th0}$, where $E_{th0} \approx 32$ kV/cm and $\eta(h) = N(h)/N_0$ is the scaling factor (N_0 is the air density at sea level). However, the runaway breakdown can develop at $E \geq E_{rb} \simeq 0.1E_{th}$, provided that 'seed' MeV-electrons are supplied by cosmic rays and the size of the region exceeds $l_{rb} \simeq 50/\eta$ m (Gurevich and Zybin 2001).

Abrupt (within 17 ms) changes in the Jets' dynamics indicate rapid variations in the source (charge) that apparently are unrelated to CG flashes. L03 questioned whether the pixies might be related to compact ($l \leq 1$ km in size) IC discharges, accompanied by broadband radio emissions of a few ms duration, or to $\ll$1-ms radio bursts observed in upper portions of a cupercell (e.g., Rakov and Uman 2003). Trakhtengerts and Iudin (2005) show that strong convection flows in the developed dome can become unstable, creating 'microscale' ($l_{ms} \sim 1$ to 10s m) charged convection cells within a few minutes. The microscale electric field can reach the breakdown value E_{th} (note that $l_{ms} < l_{rb}$) and initiate a microdischarge, manifested by a $\ll$1-ms radio burst. The discharge from one micro cell triggers neighboring cells. Ultimately, a cluster of micro cells with the near-breakdown electric field can be formed, while the average field in the cloud remains well below E_{th}. The formation of such cluster near the top might initiate an upward discharge. Given all necessary conditions, the latter should occur rather rarely.

3 Modeling Jets

3.1 Basics of Transient Discharges

We outline some basic features of the streamer/leader discharges in air, relevant to our topic (e.g., Raizer 1991 (R91); Bazelyan and Raizer 1998 (BR98), 2000 (BR00)). Positive *or* negative (single-headed) streamers/leaders are initiated near an anode or cathode, transporting '+' or '−' charge toward the opposite electrode. In negative streamers, electrons drift upstream, so seed electrons are not needed. In positive streamers, electrons drift downstream and seed electrons are mainly due to photoionization by UV radiation from the front. Between electrodes, double-headed (positive *and* negative) or bi-leaders can be formed. Each head of the bi-leader develops as in the corresponding single-headed leader, while zero net charge is transported.

Developed streamers represent low-conductive cold plasma filaments growing in the applied electric field E_a, which exceeds the critical value $E_s^{(-)} \simeq 3E_s^{(+)} \simeq 0.45E_{th}$. If E_a decreases with distance, streamers can cross the gap of length d under applied voltage U_a only if the mean field $\langle E_a \rangle = U_a/d \geq E_s$. The space charge in front of the streamer tip amplifies E_a. As a result, the total field E exceeds E_{th} and drives electron avalanche. The drift (current) of newly-born electrons makes the 'old' tip the leading segment of the plasma channel, while the avalanche region becomes the 'new' charged tip. This process has the nature of a self-sustained ionization wave moving along the axis $\mathbf{z} \| \mathbf{E}_a$ at a speed $u_s = dl_s/dt$, where l_s is the streamer length. Usually, the wavefront frame of reference $\xi = z - \int_0^t u_s dt'$ is used.

Figure 4 shows a schematic of the positive streamer tip of radius r_s and spatial distributions of E, the electron density n_e, and the space charge $\rho = e(n_i - n_e)$, where e/n_i is the

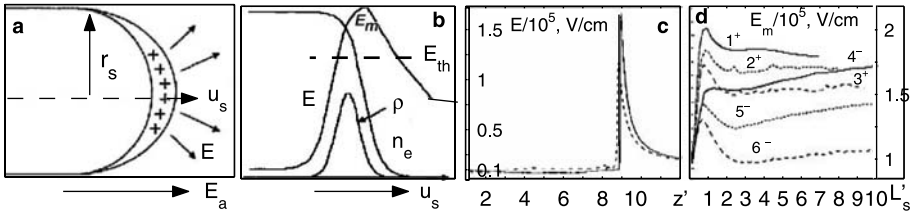

Fig. 4 Schematic of (**a**) the *spherical* tip of a positive streamer with the *cylindrical* channel of the radius r_s and (**b**) the spatial distribution of E, space charge ρ, and the electron density n_e. The *dashed line* indicates the breakdown threshold E_{th}. (**c**) The magnitude of the electric field in the positive/negative (*solid/dotted line*) streamers vs. $z' = z/r_0$ at $l_s \simeq 9r_0$. (**d**) The peak value E_m of the electric field in the positive (1^+–3^+) and negative (4^-–6^-) streamers vs. $L'_s = l_s/r_0$ (see text). The plots are adapted from Raizer et al. (1998) (**a**, **b**) and BN97 (**c**, **d**). Printed by permission from IOP Publishing Ltd. and IEEE

ion charge/density. Also shown are the results of 2D numerical simulations of *cylindrical* streamers growing along the applied field $\mathbf{E}_a \| \mathbf{z}$ from a charged sphere of radius $r_0 = 1$ mm and potential U_0 at $p = p_0$ (Babaeva and Naidis 1997 (BN97)). The total field comprises of two parts $\mathbf{E}(\mathbf{r}) = -\nabla(U_\rho + U_L)$. Here U_ρ is defined by ρ via Poisson's equation and U_L is the Laplacian potential of the charged sphere, yielding $E_{L0} = U_0/r_0 + 3E_a$ at the sphere surface and $E_L \to E_a$ at $z > 3r_0$. In the BN97 simulations $E_{L0} = 115$ kV/cm and $E_a = 15$ (frames c and d (3^+, 6^-)), 25 (2^+, 5^-), and 35 (1^+, 4^-) kV/cm. Note that $E_a = 15$ kV/cm barely exceeds $E_s^{(-)}$ and equals $\simeq 3E_s^{(+)}$.

The distribution of ρ is defined by the continuity equation $\partial\rho/\partial t + \nabla \mathbf{j}_s = 0$. Here $\mathbf{j}_s \simeq -en_e\mathbf{u}_e \simeq \sigma_e \mathbf{E}$ is the electric current density, $\mathbf{u}_e \simeq -(e\nu_{en}^{-1}/m)\mathbf{E}$, ν_{en}, and $\sigma_e = (e^2/m)n_e/\nu_{en}$ are the electron drift speed, collision frequency, and conductivity, respectively. Note that the ion motion is neglected. The narrow front width $\delta\xi_f \ll r_s$ (see Figs. 4a and 4c) makes possible simple 1D estimates of the streamer parameters (e.g., BN97; BR98). As the field is enhanced at $\xi \sim r_s$, from the electron continuity equation in the front frame it follows (e.g., BN97)

$$u_s \pm u_{em} \simeq \nu_{im} \cdot r_s / \ln(n_m/n_a). \tag{1}$$

Here the $+/-$ sign corresponds to positive/negative streamers, n_a is the electron density upstream, E_m, n_m, $\nu_{im} = \nu_i(E_m) \simeq 2.9 \cdot 10^{11}\eta \exp(-\frac{10E_{th}}{E_m})$ s^{-1}, and $u_{em} = u_e(E_m)$ are the peak values of the electric field, electron density, ionization frequency, and electron drift speed, respectively. Note that ν_i and the dielectric relaxation time $\tau_\sigma = \epsilon_0/\sigma_e$ (ϵ_0 is the permittivity of vacuum) are very sensitive to the value of E. This is a key factor in the formation of the narrow front.

For given u_s and r_s, positive streamers have greater values of E_m than negative streamers (cf. Figs. 4c, 4d). From the charge continuity equation it follows that $\rho \simeq en_e u_e/u_s \simeq \sigma_e E/u_s \ll en_e$ at $u_s \gg u_{em}$ and that the space charge lifetime is close to the relaxation time τ_{σ_m} downstream. This implies (Raizer et al. 1998 (R98)) that at least the last electron generation in the avalanche is born during this time, i.e. $\nu_{im}\tau_{\sigma_m} \gtrsim 1$ or

$$n_m \gtrsim (\epsilon_0/e)\,\alpha_m \cdot E_m \tag{2}$$

where $\alpha_m = \alpha(E_m)$ and $\alpha = \nu_i/u_e$ is the Townsend ionization coefficient.

The values of r_s and E_m are related via the potential at the charged streamer tip $\Delta U_t = U_t(l_s) - U_a(l_s) \simeq 2r_s \cdot E_m$, where the account for the conductive segment of the channel is taken (R98; BR98). Figure 4d shows that far from the launching electrode, $E_m = c_m(E_a) \cdot$

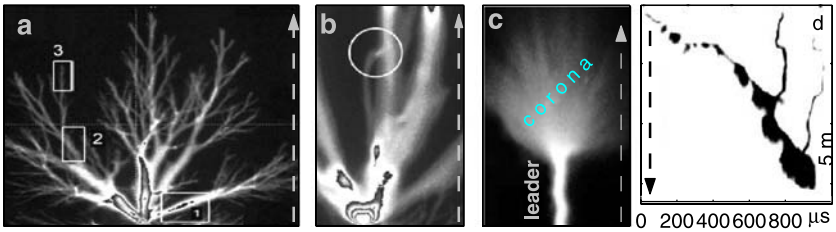

Fig. 5 (**a**, **b**) Positive streamer patterns growing from an anode in 8/4-cm gaps at atmospheric pressure and applied voltages $U_a = 60/54$-kV (adapted from Briels et al. 2006). (**c**, **d**) Examples of positive leaders (adapted from R07/ Domens et al. 1991). Reprinted by permission from the IOP Publishing Ltd. and American Geophysical Union

$E_{th} \simeq$ const. R98 argued that for the strong streamers ('*ss*'), i.e. $u_s \gg u_{em}$ or $E_a \gg E_s$, the coefficient $c_m = c_{ss} \approx 5$. For the weak streamers ('*ws*'), i.e. $u_s \gtrsim u_{em}$, we take $c_m = c_{ws} \approx 3.2$ (cf. Fig. 4d). It is worth to note that the streamer speed $u_s \propto r_s \propto \Delta U_t$ at $E_a > E_s$.

Let us pool the streamer tip parameters ($n_m/r_s/U_t/u_s$ in cm^{-3}/cm/kV/m·s^{-1}) at $E_a > E_s$ (cf. R98)

$$E_m = c_m E_{th} \cdot \eta; \quad n_m \simeq 10^{14} \cdot \eta^2; \quad r_s \simeq 0.015 c_m^{-1} \cdot \Delta U_t/\eta; \quad u_s \simeq 5\,10^4 \cdot \Delta U_t. \qquad (3)$$

We next discuss some relevant results of laboratory experiments. Figure 5(a–b) shows snapshots of positive streamers growing in a ∼15-μm-point anode-plane cathode configuration in air at normal pressure (Briels et al. 2006). Applied voltages provided $\langle E_a \rangle > E_s$, thereby streamers could cross the gap. This has not yet happened in frame *a*, where boxes labelled 1, 2, and 3 indicate streamers with radii $r_{1/2/3} \simeq 2.5/0.5/0.1$ mm. Type 1/2/3 streamers carry currents $J_{1/2/3} \simeq 20/1/0.01$ A with the current densities $j_{1/2/3} \simeq 1/3/0.5$ MA/m^2. The total current in the gap remains virtually constant, indicating that the total charge is conserved, being redistributed over the ensemble of streamers.

The observations show that the streamer radius remains virtually constant until branching, which has not yet been fully understood (e.g., Niemeyer et al. 1984; Arrayás et al. 2002). Anyway, subsequent (thinner) streamers travel shorter distances at smaller speeds. The overall range of speeds is $u_{1/2/3} \simeq 10/5/1 \cdot 10^5$ m/s. Note that $u_2/u_3 \simeq r_2/r_3$, i.e. $u_s \propto r_s$. It is likely that a ≃0.1-mm radius of type 3 streamers is close to the lower limit at normal pressure, i.e. the *minimal* radius $r_{\min}$, at which the front width $\delta\xi_f \to r_{\min}$. From (3) at $c_m = c_{ws}$ we obtain $\Delta U_{\min} \simeq 2.2$ kV and $u_{\min} \approx 10^5$ m/s, in excellent agreement with u_3. Taking $r_s = r_3$ in (2) gives $u_s^{(+)} \simeq u_{\min}$ at $c_m \simeq 1.8$, corresponding to $n_{\min} \simeq 8 \cdot 10^{11}$ cm^{-3} (the 'minimal' streamer).

In frame *b*, thick streamers have crossed the gap. After that, type 3 streamers start near the anode. Some of these late streamers merge with existing thick streamers, as shown in the circle. This (electrostatic) attraction is consequent to a 'return stroke', piercing the thick streamer and changing its polarity (Briels et al. 2006).

Developed leaders (like in Fig. 5c) represent highly conductive plasma channels, continuously emitting a fan of streamers of the same polarity, termed the streamer zone or corona. The tip moves at a speed much slower than that of individual streamers. Gas in the leader channel is heated by the current to $T \geq 1000$ K. A huge number of short-lived streamers in the corona generate the space-charge field $\langle E_c \rangle \simeq E_s$ (BR00). As streamers move along some distance until termination, their charge covers the leader channel and prevents its expansion and cooling. The overall process has not yet been fully understood, and no rigorous solution is found. Note that the average number of the coronal streamers is roughly

$d_l^2/\langle 4r_s^2\rangle \sim 10^6$–$10^9$, where d_l is the leader diameter and $\sqrt{\langle r_s^2\rangle}$ is the average streamer radius.

For positive leaders in a ∼17-m gap under voltages 2.3–2.4 MV, three types of propagation were documented: continuous (*c*), oscillatory (*o*), and restrike (*r*) (Domens et al. 1991). That the average field in the gap $\langle E_a\rangle \approx 1.4$ kV/cm is well below $E_s^{(+)}$ indicates that the high potential is transferred along the gap by the conductive leader. The length and diameter of the *c*-type leader increase smoothly with time, whereas the corona fluctuates. The speed of the leader tip is related to the dicharge current J_l as $V_l = 9.5 + 10 \cdot J_l$ km/s. Type *o* is manifested by strong sub-millisecond oscillations in the current and in the brightness of the corona and channel. However, the current never vanishes, and its mean value is close to $J_l \sim 1$ A.

Intermittent *r*-type discharges (like in Fig. 5d) develop a large bright corona. It generates the space-charge field so large that it chokes the discharge, and the current briefly vanishes. The controlling factor is the charge per unit of the leader length q_l. If q_l is too large or too small, the propagation stops due to an excess of ions (choking effect) or a lack of electrons. Ultimately, the charge per unit length of propagating leaders is nearly the same ∼50 μC/m. The discharge resumes (restrike) following the field recovery near the anode. Each restrike uses the imprint of the old leader, giving a luminous transient and a new corona (cf. rebrightenings/trailing jets in Sect. 2).

Finally, leaders of the negative polarity develop stepwise (step leader) with the time between steps ∼30–100 μs and the step length in the range of 5–200 m. There are slow α-leaders, traveling at an average speed $(1\text{–}8) \cdot 10^5$ m/s, and β-leaders that are faster and have more branches and longer steps. The electric fields required for propagation of the positive and negative leaders are nearly identical (R91).

3.2 Earlier Streamer Models of Jets

Sukhorukov et al. (1996 (S96)) and Pasko et al. (1996 (P96)) considered BJ/BS as upward streamers launched from thunderstorm tops at ∼18–20 km. Figure 6 shows a schematic of the distributions of charges and electric fields suggested for (a) negative (S96) and (b) positive (P96) *conical* streamers. This is a clear illustration of the alternatives, whatever the charge source (see Sect. 2.3). Shown next is the magnitude of the vertical electric field $E_a(h)$ from a Gaussian-shape of radius $r_0 = 3$ km thundercloud charge $Q_c = 120$ C placed at altitude $h_c = 15$ km (Pasko and George 2002 (PG02)). These conditions correspond to the cloud potential $U_c \sim Q_c/(4\pi\epsilon_0 r_0) \sim 300$ MV. Dashed lines indicate the critical field values, scaled according to $E_{th}(h) = \eta \cdot E_{th0}$ and $E_s(h) = \eta \cdot E_{s0}$ with $\eta = N/N_0 = \exp(-h/H)$ and $H \approx 7.2$ km.

Near the source $E_a > E_s^{(+)}$, thereby the positive streamer could be initiated. If the (negative) charge were located at $h_c \geq 18$ km, the negative streamer would be possible. In addition, Fig. 6d shows the nighttime atmospheric conductivity $\sigma_0(h)$ at low latitudes with values of $\tau_{\sigma_0}(h) = \epsilon_0/\sigma_0(h)$ superimposed (PG02). Clearly, if the applied field fell below E_s before the streamer arrival, it would stop shortly.

S96 suggested that the maximum field at the front (E_m) barely exceeds E_{th}, thereby the negative streamer propagates at the constant speed $u_{\min} \simeq 10^5$ m/s. As the relaxation time $\tau_{\sigma 0}$ at $h \simeq 40$ km is close to the streamer propagation time (∼0.2 s), it ultimately terminates near this altitude (cf. Fig. 1). S96 also noticed that $E_a(h)/\eta(h)$ has a minimum between 20 and 30 km (see Fig. 6c). Thus, streamers of either polarity, initiated by the 'marginal' cloud charge, cannot pass through this region, thereby becoming starters (cf. Fig. 4(a,b) PG02). However, notwithstanding $u_{\min}$ is the lower limit for the streamer speed, the value

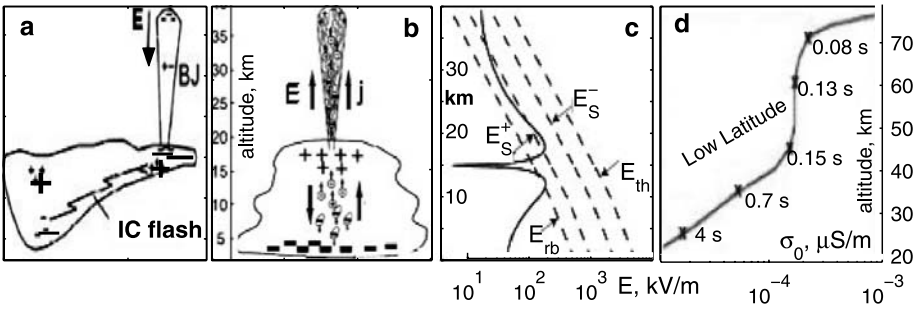

Fig. 6 Schematic of charges and electric fields for (**a**) negative and (**b**) positive streamers, respectively. (**c**) The vertical electric field (*solid line*) produced by a 120 C thundercloud charge located at $h_c = 15$ km. *Dashed lines* show E_{rb}, E_{th}, and $E_s^{(\pm)}$. (**d**) Profiles of the nighttime low-latitude atmospheric conductivity, with τ_σ superimposed. The plots are adapted from S96 (**a**), P96 (**b**), and PG02 (**c**, **d**). Printed by permission of the American Geophysical Union

$E_m \simeq E_{th}$ is too low (see Sect. 3.1). In turn, the P96 positive streamer model does not account for electron attachment and arbitrarily bounds n_m, which is hardly applicable in the stratosphere (Sukhorukov and Stubbe 1998).

The apparent shortcoming of the streamer models is that they require the large thundercloud charge (potential) to sustain the streamer propagation. Therefore, Sukhorukov and Stubbe (1998), Petrov and Petrova (1999), and PG02 suggested that BJ is rather formed by the streamer corona of an upward-growing positive leader. The leader transfers the cloud potential from its origination point $U_c(h_0) = U_c$ upward. As a result, at any altitude h_l the leader tip potential $U_l = U(h_l)$ is close to U_c and can provide the necessary voltage to support long streamers.

However, unrealistic charge transport (electric current) in the thundercloud is required to sustain a single-headed leader. Indeed, currents ≥ 1 A maintain a single steady-growing streamer. Given ~ 1 nC/m^3 density of the (attached to hydrometeorites) charge in a thundercloud (e.g., Saunders 2008), microparticles must be collected from the volume ≥ 1 km^3 and transferred into a narrow leader channel within 0.1–0.2 s. The conventional lightning theory circumvents this obstacle by applying the uncharged bi-directional leader (Kasemir 1960; Mazur and Ruhnke 1998). As the opposite-polarity leaders, propagating in opposite directions, are connected via the highly-conductive channel, their charges compensate each other. Thus, virtually no charge is taken from the cloud.

Next, we discuss the Raizer et al. (2006 (R06), 2007(R07)) model of the bi-directional leader, which describes the formation of long coronal streamers escaping into the ionosphere, alike GJ$^{(2)}$ (stage B) in Fig. 2.

3.3 Bi-leader Model of Jets

Apparently, if the bi-leader is initiated in the anvil, one of them can extend beyond the cloud top, as depicted in Fig. 7a. The bi-leader is likely triggered near the bending point B, where the vertical electric field $E_a = -dU_c/dh$ is maximum. R06 and R07 presumed an upward-propagating positive leader. However, the negative net charge in the anvil (cf. Fig. 6a) might result in the bi-leader with the negative leader upward.

Coronal streamers develop upward in the space-charge field of the corona $\langle E_c \rangle$. Its generation mechanism has not yet been quantitatively described. However, numerous experiments

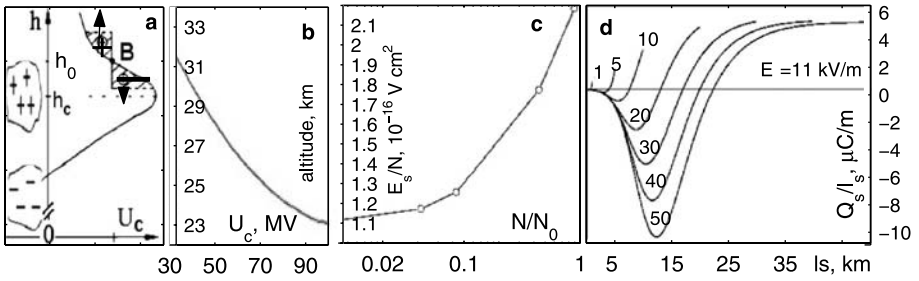

Fig. 7 (**a**) A schematic of the bi-leader initiation. (**b**) The escape altitude of a streamer from the leader tip into ionosphere vs. the cloud potential. (**c**) The critical value of $\overline{E}_s^{(+)}/N$ vs. $\eta = N/N_0$ in the exponential atmosphere. (**d**) The charge per unit length vs. the length of the positive streamer in the exponential atmosphere. Numbers 1, 5, etc. indicate the streamer length in km. The plots are adapted from R06 (**a**) and R07 (**b**–**d**). Printed by permission of the Elsevier Ltd and American Geophysical Union

established that the mean coronal field under normal conditions is close to E_{s0} (RB00). Likewise the principle of least action, in the exponential atmosphere $\langle E_c(h)\rangle$ is suggested to be close to $E_s(h) \propto \eta(h)$, i.e. just enough to maintain the streamer propagation. As a result, streamers would grow preferentially upward at small angles with the trunk, thereby forming a narrow cone (cf. Figs. 1 and 2).

R07 describe the evolution of long *conical* ($dr_s/dz \ll 1$) streamers growing from the tip of the positive upward leader by a system of equations of a long distributed line (e.g., BR00)

$$\partial q/\partial t = -\partial J/\partial z; \qquad \partial U/\partial z = -J \cdot R \tag{4}$$

and (3). Here $z = h - h_l$, J is the current in the channel, R, $q = C \cdot (U - U_a)$, and $C \approx 2\pi\epsilon_0/\ln(l_s/r_s) \simeq 8$–$10$ pF/m are the resistance, charge, and capacity per unit length of the streamer channel, respectively. The boundary condition at the base, $z = 0$, is $U(0) \simeq U_c$, whereas that at the front, $z = l_s$, relates the current and charge of the newly formed tip

$$J(l_s) = q(l_s) \cdot u_s = C \cdot (U_t - U_a) \cdot u_s. \tag{5}$$

The resistance $R(z) = (\pi r_s^2 \sigma_e)^{-1}$ is defined by the local conductivity $\sigma_e(z) \propto n_e(z)/\nu_{en}(z)$, which depends mainly on the electron attachment rate $\nu_a \simeq 1.3 \cdot 10^7 \eta^2$ s^{-1} downstream (BR98). Basically, the streamer channel is a poor conductor, except for its leading section $l_s - u_s/\nu_a < z_{sc} \le l_s$, where $n_e \simeq n_m$ (3). The R07 simulations performed in the uniform atmosphere at various densities N and applied fields E_a show that long streamers grow continuously if E_a exceeds the critical value $\overline{E}_s^{(+)}$. Figure 7c shows that at $\eta < 0.1$ or above $\simeq$17 km the ratio $\overline{E}_s^{(+)}/N$ approximately follows a scaling law $\overline{E}_s^{(+)}/N \simeq 1.3{\cdot}10^{-16}$ V cm^2, which yields $\overline{E}_{s0}^{(+)} \approx 0.65 \cdot E_{s0}^{(+)}$ (R07). At lower altitudes, electron attachment rapidly reduces the channel conductivity, thereby the similarity law is violated.

Following R06 and R07, we estimate the conditions for a streamer from the leader corona to reach the ionosphere. Let us recall that at $N = \text{const}$ and decreasing E_a, the ultimate length l_∞ of a streamer is defined by the condition $l_\infty \cdot E_s = -\int_0^{l_\infty} E_a dz = U_a$ (the applied voltage). For the leader-streamer corona system, U_a is replaced by the potential drop between the leader tip and the edge of the corona at $h_\infty = h_l + l_\infty$, i.e. $\Delta U_{ls}(h_\infty) \simeq U_c - U(h_\infty)$. As streamers stop at $\Delta U_t < \Delta U_{\min} \ll U_c$ (see Sect. 3.1), we get $\Delta U_{ls}(h_\infty) \simeq U_c - U_a(h_\infty)$, where $U_a(h_\infty)$ is the potential drop between h_∞ and the ionosphere's lower edge.

In the exponential atmosphere, integrating $E_s(h)$ over the streamer zone yields explicitly (R06)

$$\langle E_s \rangle \cdot H = U_c - U_a; \qquad \langle E_s \rangle = E_s(h_l)\,[1 - \exp(-l_\infty/H)]. \tag{6}$$

Let us assume that the front of the streamer zone is located at such distances from the ionosphere that $U_a(h_\infty) \ll U_c$. Neglecting U_a in (6) defines the altitude extent of the corona (R06)

$$l_\infty = -H \cdot \ln\bigl(1 - (E_s(h_l)\,H/U_c)^{-1}\bigr). \tag{7}$$

Apparently, the streamer zone extends indefinitely ($l_\infty \to \infty$), i.e. the streamers escape into the ionosphere, at $E_s(h_{l\infty}) = U_c/H$. This condition determines the escape altitude $h_{l\infty} = H \cdot \ln(H\,\overline{E}_{s0}/U_c)$. Figure 7b shows $h_{l\infty}^{(+)}$ as a function of U_c (R07). One can see that the positive leader tip at $h > 26$ km emits streamers that reach the ionosphere at rather moderate values of the cloud potential $U_c < 60$ MV. For comparison, the potential at the surface of a charged sphere of radius r_0 [km] and charge Q_c [C] is $U_c \simeq 10\,Q_c/r_0$ MV. Assuming the same scaling law for the negative upward leader yields the escape altitudes $h_{l\infty}^{(-)} = h_{l\infty}^{(+)} + H \cdot \ln(\overline{E}_{s0}^{(-)}/\overline{E}_{s0}^{(+)}) \approx h_{l\infty}^{(+)} + 8$ km.

We suggest that the escape altitude is also the terminal altitude of the leader, since the escaping streamer would likely cause the return stroke from the ionosphere and temporarily discharge the gap, likewise CG flashes. This conjecture is in good agreement with Fig. 2 (stage B), where the trunk top is near 30–35 km.

Figure 7d shows the charge distribution per unit channel of the positive streamer growing in the exponential atmosphere under the applied electric field $E_a(h) \propto \overline{E}_s^{(+)}(h)$ (R07). The streamer starts from the leader tip at $h_l = 25.2$ km, where the applied field $E_a(h_l) = 11.0$ kV/m is slightly above $\overline{E}_s^{(+)}(h_l) = 10.6$ kV/m. Apparently, substantial negative charges are generated in the trailing part of the channel, though the net charge is positive. This is the consequence of the long streamer length (BR98). Indeed, as the applied field moves electrons further downstream, the positive charge is accumulated in the streamer tip. As long as the streamer channel is short and the electron attachment is negligible, the current flows through the whole channel 'freely'. As soon as the conductivity reduces near the base ($\nu_a \propto N^2$), the channel plasma polarizes in order to maintain the current.

Note that this type of the charge distribution can cause the electrostatic attraction of the tip of the later streamer to the trailing part of the earlier streamer, irrespective of the streamer (net) polarity (cf. Fig. 2).

4 Jets Observables

4.1 Optical Emissions

The upward-growing leader channel represents the bright white trunk of Jets, whereas the coronal streamers form branches and a faint 'flame' near the terminus. First, let us estimate the radiation of the trunk. The energy flux from unit volume of heated air of the temperature T [K] is given by $\Phi_\varepsilon = \kappa\sigma_T T^4$, where σ_T is the Stefan constant and $\kappa = 2 \cdot 10^{-13} T^3 \cdot \eta^{3/2}$ m^{-1} is the inverse characteristic length (Gurevich et al. 1997). Then, the column emission rate, the surface brightness in Rayleighs (megaphoton $\cdot$ cm^{-2} s^{-1}), is found by integrating Φ_ε along the line of sight

$$I_l \simeq (4\pi\,\varepsilon_\lambda 10^6)^{-1} \kappa\,\sigma_T T^4 d_l \quad [\mathrm{R}] \tag{8}$$

(ε_λ is the mean energy of the radiated photons of the wavelength λ). At $T = 1000$ K, $\varepsilon_\lambda \sim 10$ eV, and the leader diameter $d_l \sim 100$ m, Eq. (8) yields $I_l \sim 15$ MR at altitudes $\sim$30 km (cf. W01).

Let us estimate the intensity of optical emissions from the coronal streamers. The main contributors to the red- and blue-line emissions are known to be the first (1PN2) and second (2PN2) positive bands of molecular nitrogen, respectively. Besides, $\simeq$2.3% of the N_2 ionization radiates in the band 1NN2+ at $\lambda = 427.8$ nm (Vallance-Jones 1974). Likewise ionization, the excitation rates, ν_λ, are very sensitive to the value of E/N (R91), thereby the front region with $E \to E_m = c_m E_{th}$ is most luminous. As $E_m/N = \text{const}(h)$, the value of ν_λ varies as $\propto N$, until the streamer slows down and E_m falls. To estimate the brightness of the fast-moving tip of a streamer, the limited excitation time must be accounted for

$$I_\lambda \simeq (4\pi 10^6)^{-1} \Delta r_\parallel n_{em} \nu_\lambda [1 - \exp(-\tau_f/\tau_\lambda)]/(1 + A_\lambda^{-1} k_\lambda N) \quad \text{[R]}. \tag{9}$$

Here $\Delta r_\parallel \sim r_s$ is the glow dimension along the line of sight, $\tau_\lambda = (A_\lambda + k_\lambda N)^{-1}$ is the lifetime of excited quanta, $A_2 \approx 120 A_1 \approx 1.4 A_+ \approx 2 \cdot 10^7$ s^{-1} and $k_1 \approx 1.4 k_2 \approx 0.25 k_+ \approx 10^{-10}$ cm^3 s^{-1} are the radiation probabilities and quenching rates, respectively (Vallance-Jones 1974), and $\tau_f \sim \alpha_m^{-1}/u_s$ is the front transit time. Hereafter, subscripts '+', '1', and '2' indicate 1NN2+, 1PN2, and 2PN2, respectively.

As $\nu_1 \sim \nu_2$ at $E > E_{th}$ and $A_1 \ll A_2$, the blue-line emissions dominate, thereby setting the blue color of Jets. Evidently, the luminosity range is set up by the parameters for the strong and minimal streamers with the excitation rates $\nu_2^{(ss)} \approx 5 \cdot \nu_+^{(ss)} \approx 5 \cdot 10^{10} \eta$ s^{-1} and $\nu_2^{(\min)} \approx 100 \cdot \nu_+^{(\min)}$, respectively (Fig. 3a PG02). An ideal event to compare with is the EXL98 starter, where the reported intensity I_+ and the ratio I_+/I_2 in the brightest part are about 10 kR and 0.01, respectively (W01). Let us presume that the starter terminated at $20 \le h_t \le 25$ km, where $0.05 \le \eta_t \le 0.03$ and $\tau_f^{(\min)} \gg \tau_\lambda \gg \tau_f^{(ss)}$. For the strong streamers (9) reduces to $I_\lambda^{(ss)} \simeq 10^{-7} n_{em} r_s \tau_f \cdot A_\lambda \nu_\lambda^{(ss)}$, giving the ratio $I_+^{(ss)}/I_2^{(ss)} \simeq 1/7$, which greatly exceeds the observed ratio. The opposite is true for the minimal streamer, as $\tau_+(h_t) \ll \tau_2(h_t)$.

Therefore, as anticipated, the weak streamers are characteristic of the starter corona. The sought-for ratio matches the observed value at $c_m^* \approx 2.45$, when $\tau_2^{(*)} \gg \tau_f^{(*)} > \tau_+^{(*)}$. At $\nu_+^* \approx 10^9 \eta$ s^{-1} (Fig. 3a PG02), $r_s^* \sim 5 \cdot 10^{-2}/\eta$ cm, and $n_{em}^* \approx 10^{12} \eta^2$ cm^{-3}, from (9) we get the 'instant' brightness of the streamer tip $I_+(h_t) \simeq 120$ MR (cf. Stenbaek-Nielsen et al. 2007). The coronal glow dimension in the exponential atmosphere is of the order of d_l (implying the cone angle $\le$15°). The 'instant' radiating layer, i.e. the path $\xi_\lambda = u_s/A_\lambda \sim 1$ cm, covered by the front within the radiation time, is much smaller than the size of one pixel, say, $l_0 \sim 10^2$ m. Reducing the radiated flux $I_+(h_t)$ by a factor $\xi_+ d_l/l_0^2 \sim 10^{-4}$ yields 12 kR, in fair agreement with the observed value. Note that the total blue-line radiation power from a single streamer amounts to $\sim$0.1 MW/m^3, whereas that from the whole corona $\sim$3 TW/m^3.

4.2 Long-Lived Effects of Jets in the Stratosphere

4.2.1 Ozone Layer Perturbations

Sentman and Wescott (1996) suggested that upward discharges might create long-lived by-products and thus have long term consequences in the atmosphere. In particular, Jets crossing the ozone layer can affect its chemical composition. In the stratosphere, nitric oxide

(NO) and dioxide (NO_2) molecules are known to limit the content of ozone due to the reactions (Crutzen 1970)

$$NO_2 + O \rightarrow NO + O_2; \qquad N + O_2 \rightarrow NO + O; \qquad NO + O_3 \rightarrow NO_2 + O_2. \tag{10}$$

As the rate coefficients of the last two reactions sharply increase with T, the NO production and O_3 destruction by an ordinary lightning is based on the heating of gas up to $T \geq 1000$ K (Lawrens et al. 1995). This scheme is hardly applicable for streamers, as the gas temperature in the front is virtually unchanged (Mishin 1997). However, ionization and dissociation by energetic electrons in discharges trigger the chain of chemical reactions resulting in NO and O_3 perturbations (e.g., Kossyi et al. 1992).

Mishin (1997) and Smirnova et al. (2003) explored a plasmochemical model to study NO and O_3 perturbations in the front (tip) of a negative streamer. Besides the basic reactions (10), the model includes electron impact ionization, excitation, and dissociation processes, along with dissociative recombination and charge exchange (Kossyi et al. 1992). Using the (underestimated) streamer parameters from the S96 model, they found that local perturbations of NO (O_3) by a single Jet amount to tens (tenths) per cent and last for a few minutes.

A fairly accurate estimate of the NO perturbation can be derived from the power dissipated in the front, $W_f \sim \sigma_e E_m^2$. As the energy needed to create one NO molecule is $\Delta\varepsilon \sim 50$ eV (Kochetov et al. 1986), one gets $[NO]_{max} \sim W_f/\Delta\varepsilon \cdot r_s/u_s$ (Mishin 1997). Using the streamer tip parameters from (3) yields $W_f \sim 10 \cdot \eta^3$ MW/cm^3 and $[NO]_{max} \sim 10^{14}\eta^2 \sim 10^{11}$ cm^{-3} at 25 km, which well exceeds the background NO content. In the leader-corona system, the composition of the heated gas in the leader channel is affected due to the basic reactions (10). Additionally, NO, NO_2, and O components can be produced by the streamer coronal. At $T \sim 1000$ K, Eq. (10) predicts that the O_3 content inside the leader at 20–30 km depletes by an order of magnitude within ~20–50 ms. However, only numerical modeling can account for every possible reaction to give accurate predictions. Finally, vibrationally-excited NO molecules radiate in the infrared band at 5.3 μm (the time const ≈ 12 s). Simple estimates show that the emitting layer of 10 km and $[NO] \sim 10^{11}$ cm^{-3} yields the energy flux ~10 W/m^2, well above the strongest infrared fluxes from the auroral zone.

4.2.2 Conductivity Perturbations and Effects

Holtzworth and Hu (1995) suggested that Jet-associated conductivity perturbations might be significant for the global electric circuit. Indeed, Sukhorukov and Stubbe (1998) estimated that during the final phase Jets represent conducting channels, short-circuiting the gap between the thundercloud top and ionosphere. They stressed that the plasma in the channel decays slowly, supporting the conductivity perturbation for much longer time after the optical emission ceases. This conjecture agrees well with the Lehtinen and Inan (2007) modeling, showing that gigantic jets leave the ionization trail above 50–60 km, which lasts for a few minutes.

The persistence of highly-conductive 'wires' will discharge (charge) the ionosphere in the case of upward transfer of the negative (positive) charge. Anyway, the thundercloud charge will be reduced. For example, ~300-A currents remove ~30 C within ~0.1 s. This effect might be responsible for the reported temporary decrease of the local lightning activity after occurrence of a blue jet/starter (Sect. 2.3). Furthermore, as the electron density decays much faster at lower altitudes (Sect. 3.3 and Fig. 2 (Lehtinen and Inan 2007)), the conductivity below ~50 km virtually recovers, whilst that at higher altitudes remains greater

than the background. This implies that the effective 'ionospheric' boundary is moved down to 50–60 km, thereby explaining the altitude extent of the trailing jets and their bright tops (Fig. 2).

5 Conclusion

We describe the salient features of upward discharges (Jets) in the atmosphere. The state-of-the-art in theoretical and laboratory modeling of transient discharges in air pertinent the physics of Jets is outlined. An assessment of the models of the blue jet development is given. The bi-directional leader concept seems to explain the basic features of Jets. The possible role of Jets in the electrodynamics and chemistry of the middle atmosphere is discussed.

Acknowledgements EVM thanks the International Space Science Institute for its hospitality during this Workshop as also the authors of the contributions contained in the chapter on electric discharges. Work by EVM is partly supported by AFRL contract FA8718-04-C-0055 with Boston College. Dr. Hsiu is acknowledged for sending the original movie of one of the gigantic jets.

References

M. Arrayás, U. Ebert, W. Hundsdorfer, Phys. Rev. Lett. **88**, 174502-1–174502-4 (2002).
N. Babaeva, G. Naidis, IEEE Trans. Plasma Sci. **25**, 375 (1997)
E. Bazelyan, Y. Raizer, *Spark Discharge* (CRC Press, Boca Raton, 1998)
E. Bazelyan, Y. Raizer, *Lightning Physics and Lightning Protection* (IOP Publishing, Bristol, 2000)
T. Briels, J. Kos, E. van Veldhuizen et al., Appl. Phys. D **39**, 5201 (2006)
W. Boeck, O. Vaughan, R. Blakeslee et al., J. Geophys. Res. **100**, 1465 (1995)
W. Boeck, O. Vaughan, R. Blakeslee et al., J. Atm. Sol. Terr. Phys. **60**, 669 (1998)
P. Crutzen, Quart. J.R. Met. Soc. **96**, 320 (1970)
S. Cummer, N. Jaugey, J. Li, W. Lyons et al., Geophys. Res. Lett. **33**, L04104 (2006). doi:10.1029/2005GL024969
P. Domens, A. Gibert, J. Dupuy et al., Appl. Phys. D **24**, 1748 (1991)
R. Franz, R. Nemzek, J. Winckler, Science **249**(4964), 48051 (1990)
G. Garipov, M. Panasyuk, V. Tulupov et al., JETP Lett. **82**, 185 (2005)
A. Gurevich, N. Borisov, G. Milikh, *Physics of Microwave Discharge. Artificially Ionized Regions in the Atmosphere* (Gordon and Breach, Reading, 1997)
A. Gurevich, K. Zybin, Physics-Uspekhi **44**, 1119 (2001)
R. Holtzworth, H. Hu, Adv. Space Res. **16**(5), 131 (1995)
H. Kasemir, J. Geophys. Res. **65**, 1873 (1960)
I. Kochetov, E. Mishin, V. Telegin, Sov. Phys. Doklady **31**, 990 (1986)
I. Kossyi, A. Kostinsky, A. Matveyev et al., Plasma Sources Sci. Technol. **1**, 207 (1992)
M. Lawrens, W. Chameides, P. Kasibhata et al., in *Handbook of Atmospheric Electrodynamics,* vol. 1, ed. by H. Volland (CRC Press, Boca Raton, 1995), p. 189
N. Lehtinen, U. Inan, Geophys. Res. Lett. **35**, L08804 (2007). doi:10.1029/2006GL029051
W. Lyons, Geophys. Res. Lett. **21**, 875 (1994)
W. Lyons, M. Stanley, T. Nelson et al., EOS **81**, F131 (2000)
W. Lyons, T. Nelson, R. Armstrong et al., Bull. Am. Meteorol. Soc. **84**, 445 (2003)
V. Mazur, L. Ruhnke, J. Geophys. Res. **103**, 23299 (1998)
E. Mishin, Geophys. Res. Lett. **24**, 1919 (1997)
L. Niemeyer, L. Pietronero, H. Wiesmann, Phys. Rev. Lett. **52**, 1033 (1984)
V. Pasko, M. Stanley, J. Mathews et al., Nature **416**, 152 (2002)
V. Pasko, J. George, J. Geophys. Res. **107**(23299), 1458 (2002). doi:10.1029/2002JA009473
V. Pasko, U. Inan, T. Bell, Geophys. Res. Lett. **23**, 301 (1996)
N. Petrov, G. Petrova, Tech. Phys. **44**, 472 (1999)
Y. Raizer, *Gas Discharge Physics* (Springer, Berlin, 1991)
Y. Raizer, G. Milikh, M. Shneider et al., Appl. Phys. D **31**, 3255 (1998)
Y. Raizer, G. Milikh, M. Shneider, Geophys. Res. Lett. **33**, L23801 (2006). doi:10.1029/2006GL027697

Y. Raizer, G. Milikh, M. Shneider, J. Atm. Sol. Terr. Phys. **69**, 925 (2007)
V. Rakov, M. Uman, *Lightning: Physics and Effects* (Cambridge, Cambridge, 2003)
R. Roussel-Dupré, A. Gurevich, J. Geophys. Res. **101**, 2297 (1996)
H. Rowland, J. Atmos. Sol. Terr. Phys. **60**, 831 (1998)
C. Saunders, Space Sci. Rev. (2008, this issue)
D. Sentman, E. Wescott, Geophys. Res. Lett. **20**, 2857 (1993)
D. Sentman, E. Wescott, EOS Trans., AGU **77**, 1 (1996)
D. Sentman, E. Wescott, D. Osborne et al., Geophys. Res. Lett. **22**, 1205 (1995)
N. Smirnova, A. Lyakhov, S. Kozlov, Int. J. Geom. Aeron. **3**, 281 (2003)
H. Stenbaek-Nielsen, M. McHarg, T. Kanmae et al., Geophys. Res. Lett. **34**, L11105 (2007). doi:10.1029/2007GL029881
M. Stoltzenburg, T. Marshal, Space Sci. Rev. (2008, this issue). doi:10.1007/s11214-008-9338-z
H. Su, R. Hsu, A. Chen, Y. Wang et al., Nature **423**, 974 (2003)
A. Sukhorukov, E. Mishin, P. Stubbe et al., Geophys. Res. Lett. **23**, 1625 (1996)
A. Sukhorukov, P. Stubbe, J. Atmos. Sol. Terr. Phys. **60**, 725 (1998)
V. Trakhtengerts, D. Iudin, Radiophys. Quant. Electron. **48**, 720 (2005)
A. Vallance-Jones, *Aurora* (Reidel, Dordrecht, 1974)
O. Vaughan Jr., B. Vonnegut, J. Geophys. Res. **94**, 13179 (1989)
O. Vaughan Jr., R. Blakeslee, W. Boeck et al., Mon. Weather Rev. **120**(7), 1459 (1992)
E. Wescott, D. Sentman, D. Osborne et al., Geophys. Res. Lett. **22**, 1209 (1995)
E. Wescott, D. Sentman, M. Heavner et al., Geophys. Res. Lett. **23**, 2153 (1996)
E. Wescott, D. Sentman, M. Heaver et al., J. Atm. Sol. Terr. Phys. **60**, 713 (1998)
E. Wescott, D. Sentman, H. Stenbaek-Nielsen et al., J. Geophys. Res. **106**, 21549 (2001)